



Optimizing Parabolic Through Collectors for Solar Stills: A 2D CFD Parametric Analysis

Mammar Bouhelal^{1,2*}, Amar Rouag^{3,4}, Abdelhamid Bouhelal⁵, Yousef Belloufi⁶

¹ Department of Mechanical Engineering, University of Kasdi Merbah, Ouargla, ALGERIA

² Laboratoire de Mécanique Appliquée et Systèmes Energétiques, Ouargla, ALGERIA

³ Department of Renewable Energies, University of Kasdi Merbah, Ouargla, ALGERIA

⁴ Laboratoire de Génie Energétique et Matériaux, University of Biskra, ALGERIA

⁵ Laboratory of Green and Mechanical Development (LGMD), École Nationale Polytechnique, Algiers, ALGERIA

⁶ Laboratoire de Génie Mécanique, Université de Biskra, ALGERIA

*Corresponding author E-mail address: bouhelal.mammar@univ-ouargla.dz

Abstract – The thermal efficiency of parabolic trough collectors (PTCs) is influenced by various parameters, including length, diameter, and mass flow rate. This study employs 2D steady-state Computational Fluid Dynamics (CFD) simulations to investigate heat transfer within PTCs and enhance their performance. Exploring diverse PTC designs, involving variations in length ($L = 0.5$ to 3 m) and diameter ($D = 10$ to 60 mm), sourced from existing research to optimize desalination system applications. The investigation covers both laminar and turbulent regimes with fully developed flows, examining the effects of Reynolds number and mass flow rate. The results highlight that collector diameter has the most pronounced impact on thermal efficiency, followed by mass flow rate, while the effect of length can be neglected in comparison. A 50% diameter increase leads to over a 60% rise in efficiency for both laminar and turbulent cases, whereas a 60% decrease in mass flow rate corresponds to a 50% enhancement and a 60% improvement in efficiency for both regimes. These findings suggest that an optimal PTC design should prioritize a smaller diameter and lower mass flow rate, with length being of secondary importance and application-specific considerations also playing a pivotal role.

Keywords: Solar energy, Parabolic trough collector (PTC), Computational fluid dynamics (CFD), Thermal efficiency, Parametric Optimization.

Received: 13/09/2023 – Revised: 24/10/2023 - Accepted: 04/11/2023

I. Introduction

In the context of mounting concerns regarding climate change and finite fossil fuel reserves, renewable energy has gained pivotal importance within the global energy landscape, offering sustainable and eco-friendly solutions. Parabolic trough collectors (PTCs), among various renewable technologies, have garnered significant attention due to their exceptional ability to efficiently harness solar energy. This surge in renewable energy adoption, as evidenced by the International

Renewable Energy Agency's 2021 report [1], has contributed about 26% to the global electricity generation capacity, mitigating the release of around 2.6 gigatons of carbon dioxide annually. This transition to renewables is driven not only by environmental considerations but also by their compelling economic advantages, underscored by decreasing technology costs and scalability, which render them increasingly competitive against conventional fossil fuel-based power generation.



In recent years, PTCs have gained prominence for their potential in electricity generation, process heat applications, and other industrial processes. Despite their promising benefits, improving the thermal efficiency of PTCs remains a critical research area [2]. Enhanced thermal performance leads to increased energy capture, reduced energy losses, and improved overall system efficiency, all of which are crucial for maximizing the economic viability and environmental sustainability of solar thermal technologies.

The optimization of PTCs poses a complex challenge due to the intricate interplay of multiple design and operating parameters. These parameters include the collector's length, diameter, receiver tube and mirror properties, receiver fluid properties, solar concentration ratio, and mass flow rate [3]. Manipulating these parameters to achieve the best thermal performance requires a comprehensive understanding of the underlying heat transfer and fluid flow mechanisms occurring within the collector.

Traditional experimental studies provide valuable insights into the behavior of PTCs, but they can be time-consuming, expensive, and limited in exploring a wide range of design possibilities [4]. In this context, Computational Fluid Dynamics (CFD) emerges as a powerful tool for simulating and analyzing the intricate fluid dynamics and heat transfer phenomena within PTCs. CFD simulations enable researchers to visualize and quantify the thermal performance of PTCs under various operating conditions, offering valuable information that can inform the design process and optimize the collectors' efficiency [5].

This paper delves into the potential enhancement of PTC efficiency through CFD simulations, with a specific focus on their application in solar desalination [6].

To achieve this goal, a two-dimensional (2D) steady-state CFD approach is employed to model the heat transfer and fluid flow processes within the PTCs. The steady-state assumption is justified, as reported in several previous works [7-9], as the dynamic response times of PTCs are much longer than the time scales of interest in most applications.

The key advantages of using CFD in this study are manifold. First, CFD provides a detailed and quantitative understanding of the complex flow patterns and heat transfer behavior inside the PTCs, which is challenging to achieve through experimental techniques alone. Second, CFD enables the exploration of a wide range of design and operating parameters in a cost-effective and timely manner. Third, the flexibility of CFD simulations allows us to gain insights into the impact of individual parameters while holding others constant, facilitating a

parametric optimization study.

The solar destination presents a straightforward, cost-effective, and environmentally friendly approach. It involves harnessing solar energy to heat water within a solar distiller, ultimately yielding pure water through the processes of evaporation and condensation. While this system has a modest production rate, global researchers are actively exploring various methods to enhance its efficiency in producing pure water.

Elevating water temperature stands out as an effective means to boost the overall performance of the solar still. To achieve this, researchers have incorporated materials such as high thermal conductivity zinc, copper, aluminum, and other elements. Additionally, they have experimented with materials like stones, gravel, and sand, among others [10-13]. The inclusion of refractors and the exploration of biological and chemical materials have been explored, all without resorting to non-particle technology [14-20].

A notable advancement involves integrating a solar collector with a solar still. This innovative approach effectively raises water temperature within the distiller without the need for materials immersed in the water. This integration proves to be a promising avenue for enhancing distiller output.

The primary objective of this research is to employ CFD simulations to conduct a systematic investigation into the impact of varying geometric and operational parameters on the thermal efficiency of PTCs for solar desalination applications. By exploring the effects of PTC length, diameter, and mass flow rate, we aim to identify the optimal configurations that maximize the solar energy capture and minimize energy losses. The subsequent sections of this article will delve into the mathematical model, numerical method, and simulation setup used for the CFD analysis. The results and discussions will then present a comprehensive evaluation of the thermal performance of PTCs under different parametric conditions.

II. Mathematical Model

The geometry under investigation, as illustrated in Figure 1, involves a two-dimensional and symmetrical rectangular tube with a varying diameter, D (0.06, 0.045, 0.025, 0.010 meters), and a changing length, L (3, 2, 1.5, 0.5 meters). These parameters were chosen based on the analysis provided by reference [21], which explored commonly utilized PTC dimensions for desalination applications.

As indicated in Figure 1, only the PTC receiver tube will be simulated. The effect of the solar concentration heat flux will be considered as a boundary condition applied on the wall surface of the PTC tube.

Two Reynolds numbers will be considered in this study; laminar case ($Re = 300$) and turbulent case ($Re = 20000$). These two Reynolds numbers have been selected to ensure the attainment of fully developed conditions. The working fluid (heat transfer fluid) is the water.

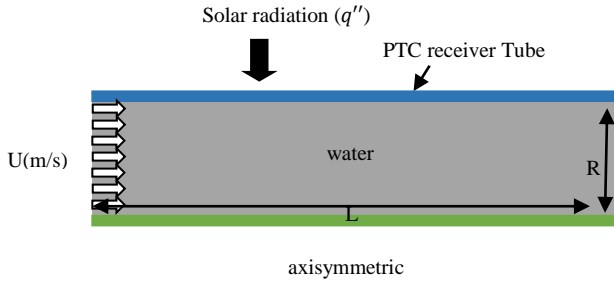


Figure 1. Dimensions of the studied PTC

At the outset, we maintain a constant length while altering the diameter in both scenarios, encompassing both laminar and turbulent Reynolds regimes. Subsequently, we adjust the diameter and replicate the identical procedure. The specific geometric measurements of the tube employed in this research are outlined in Table 1. This study assumes the fluid flow through the PTC to be steady-state, incompressible, viscous, and characterized by constant properties. As a result, the governing CFD equations are as follows [22, 23]:

Table 1. Studied geometric dimensions

Parameter	Value
Length, L (m)	3; 2; 1.5; 0.5
Diameter, D (mm)	60; 45; 25; 10
Reynolds number, Re	300; 20000
Solar radiation, q'' (W/m^2)	50000

II.1. Continuity Equation

The continuity equation stems from the principle of mass conservation and is mathematically formulated, particularly in the context of steady flow, as follows:

$$\frac{\partial u}{\partial x} + \frac{\partial v}{\partial y} = 0 \quad (1)$$

u and v represent the velocity components in the x and y directions, respectively.

II.2. Momentum Equations

Utilizing the principle of momentum conservation, connections between fluid properties, motion, and propelling forces can be established.

Under assumptions of fluid continuity, isotropy, homogeneity, and adherence to Newtonian behavior, the equations governing stationary momentum are as follows:

$$\rho \left(\frac{\partial(uu)}{\partial x} + \frac{\partial(vu)}{\partial y} \right) = -\frac{\partial p}{\partial x} + \mu \left(\frac{\partial^2 u}{\partial x^2} + \frac{\partial^2 u}{\partial y^2} \right) \quad (2)$$

$$\rho \left(\frac{\partial(uv)}{\partial x} + \frac{\partial(vv)}{\partial y} \right) = -\frac{\partial p}{\partial y} + \mu \left(\frac{\partial^2 v}{\partial x^2} + \frac{\partial^2 v}{\partial y^2} \right) \quad (3)$$

ρ and μ are respectively the density and viscosity of the fluid, p is the pressure.

II.3. Energy Equation

The energy equation is derived from the principle of energy conservation and is formulated as follows:

$$\rho C_p \left(\frac{\partial(uT)}{\partial x} + \frac{\partial(vT)}{\partial y} \right) = \frac{\partial}{\partial x} \left[k \frac{\partial T}{\partial x} \right] + \frac{\partial}{\partial y} \left[k \frac{\partial T}{\partial y} \right] + \frac{\partial}{\partial z} \left[\left(\frac{\mu}{Pr} \right) \frac{\partial T}{\partial z} \right] + \mu \left[2 \left(\frac{\partial u}{\partial x} \right)^2 + 2 \left(\frac{\partial v}{\partial y} \right)^2 + \left(\frac{\partial u}{\partial y} + \frac{\partial v}{\partial x} \right)^2 \right] \quad (4)$$

T is the temperature, k is the fluid conductivity and C_p is the specific heat capacity at constant pressure.

Equations (1) through (4) are implemented for the laminar regime. In the turbulent case, the RNG $k-\epsilon$ turbulence model [13] has been employed.

In the RNG $k-\epsilon$ model, the turbulent (or eddy) viscosity is modeled as:

$$\mu_t = \rho C_\mu \frac{k^2}{\epsilon} \quad (5)$$

The turbulent kinetic energy (k) is obtained from the following transport equation:

$$\frac{\partial(\rho k)}{\partial t} + \frac{\partial(\rho k u_i)}{\partial x_i} = \frac{\partial}{\partial x_j} \left[\left(\mu + \frac{\mu_t}{\sigma_k} \right) \frac{\partial k}{\partial x_j} \right] + G_k - \rho \epsilon \quad (6)$$

The production of turbulent kinetic energy G_k is modeled as:

$$G_k = -\rho \overline{u'_i u'_j} \frac{\partial u_j}{\partial x_i} \quad (7)$$

The transport equation for the dissipation rate of the turbulent kinetic energy (ϵ) is given by:

$$\frac{\partial(\rho \epsilon)}{\partial t} + \frac{\partial(\rho \epsilon u_i)}{\partial x_i} = \frac{\partial}{\partial x_j} \left[\left(\mu + \frac{\mu_t}{\sigma_\epsilon} \right) \frac{\partial \epsilon}{\partial x_j} \right] + C_{1\epsilon} \frac{\epsilon}{k} G_k - C_{2\epsilon} \rho \frac{\epsilon^2}{k} \quad (8)$$

Where

$$C_{2\epsilon}^* = C_{2\epsilon} + \frac{C_\mu \eta^3 (1 - \eta/\eta_0)}{1 + \beta \eta^3} \quad (9)$$

$$\eta = k(2S_{ij}S_{ij})^{1/2} / \epsilon \quad (10)$$

The constants of the model are [24, 25]:

$$C_{1\epsilon} = 1.42, C_{2\epsilon} = 1.68, \sigma_k = \sigma_\epsilon = 1.393, \eta_0 = 4.38, \beta = 0.012 \quad (11)$$

The local Nusselt number (Nu) on the PTC receiver tube is calculated using the following expression [26]:

$$Nu = \frac{q'' D}{k (T_w - T_m)} \quad (12)$$

T_w is the temperature at the wall surface, and T_m is the average temperature of the fluid in a given x location, which is calculated by:

$$T_m = \frac{\int_0^R uT(2\pi r)dr}{\int_0^R u(2\pi r)dr} \quad (13)$$

r is the local radius of the PTC tube.

The average (or mean) Nusselt number (Nu_m) is calculated from the entrance length (L_e) using the following expression:

$$Nu_m = \frac{1}{L - L_e} \sum_{i=L_e}^L Nu_i \quad (14)$$

The proprieties of the water are presented in Table 2.

Table 2. Proprieties of the heat transfer fluid (water) [15]

Property	Value
Density, ρ (kg/m^3)	998.2
Viscosity, μ ($Pa.s$)	0.001003
Thermal conductivity, k ($W/m.K$)	0.60
Specific heat capacity, C_p ($J/kg.K$)	4182

III. Numerical Method

In this study, the governing equations are numerically solved using the finite volume-based method within the ANSYS Fluent software (Academic version 2023). To solve the discretized equations, it's necessary to define dynamic and thermal boundary conditions at the boundaries of the computational domain. These conditions are summarized in Figure 2.

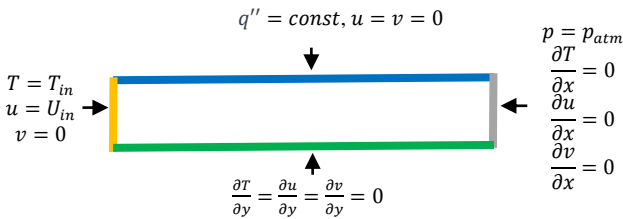


Figure 2. Applied boundary conditions.

At the inlet of the computational domain, a constant axial velocity is imposed, and a uniform water temperature of $T_{in} = 80 \text{ }^\circ\text{C}$ has been applied. While at the outlet, atmospheric pressure is maintained. On the PTC receiver wall, a constant solar radiation heat flux (q'') is applied. For the laminar cases, the non-slip condition is applied,

while for the turbulent cases, the standard wall function [27] has been used.

The Coupled Algorithm has been used for the coupling between velocity and pressure. The second-order scheme was opted for the pressure interpolation. As for the discretization schemes for the momentum and energy conservation equations, a second-order Upwind discretization scheme was selected across all transport equations. Additionally, to ensure good convergence accuracy, a value of approximately 10^{-5} was chosen for all variables except for energy, for which a value around 10^{-6} was adopted to enhance precision in modeling the heat transfer phenomenon.

The simulation was conducted on a PC equipped with 12 GB RAM and an i5-4570T CPU @ 2.90GHz. Subsequently, the outcomes were analyzed and visualized using MATLAB software to generate graphical representations.

A total of 38 simulations were carried out, encompassing six cases for the mesh independence study and four distinct combinations of lengths and diameters for each Reynolds number.

IV. Results and Discussion

In this section, we will present the simulation results obtained using the CFD code (Ansys Fluent). Firstly, we will demonstrate the mesh independence on the numerical calculation results, and we will also compare the numerically obtained results with analytically calculated ones to validate our numerical simulation. Subsequently, we will examine the impact of several parameters on the thermal performance of the studied PTC, such as:

- The influence of the PTC receiver tube length ($L = 0.5$ to 3 m).
- The influence of the PTC receiver diameter ($D = 10$ to 60 mm).
- The influence of mass flow rate or Reynolds number (laminar $Re = 300$, and turbulent $Re = 20000$).

IV.1. Mesh Independence Study

Studying the mesh independence concerning calculation results is an essential step that allows us to determine an appropriate number of elements for a successful parametric study. To achieve this, a range of mesh configurations was taken into account. The considered mesh elements include 1600, 2500, 10000, 22500, 40000, and 62500, which respectively correspond

to a uniformly structured grid of $\Delta x = \Delta y = 7.5, 6, 3, 2, 1.5,$ and 1.2 mm.

As shown in Figure 3, the average Nusselt number decreases with an increasing number of nodes. Starting from a mesh size of 36750 elements, the variation in the Nusselt number becomes stable with mesh refinement. Therefore, this specific mesh size (36750 elements), containing 37206 nodes, was selected. Its corresponding spacing ($\Delta x = \Delta y = 2$ mm) has been consistently employed for all simulations detailed in this article.

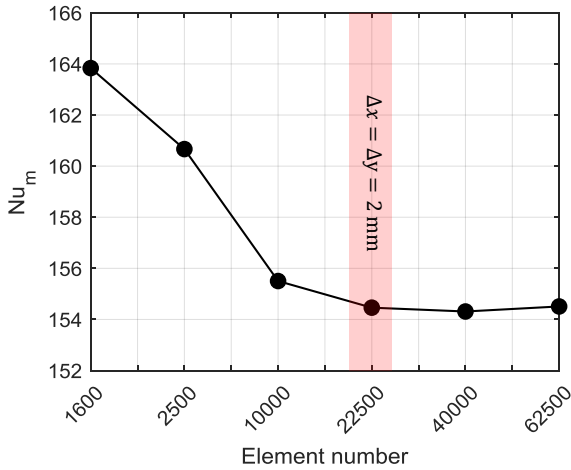


Figure 3. Mesh independence study: mean Nusselt number vs Mesh element number for $Re = 20000, L = 3$ m and $D = 60$ mm

IV.2. Numerical Validation

Following the mesh selection, the subsequent objective is the validation of CFD outcomes against theoretical predictions. It is established that the Average Nusselt number for laminar flows within pipes exposed to a uniform heat flux theoretically equates to 4.36 [15]. Conversely, for turbulent flows, no analytical formula exists, necessitating the utilization of empirical correlations. In this investigation, the widely recognized Gnielinski correlation for turbulent flows in pipes is employed [16]:

$$Nu_m = \frac{[Re - 1000].Pr.f/8}{1 + 12.7.(Pr^{2/3} - 1)\sqrt{f/8}} \quad (15)$$

Where $Pr = C_p\mu/k$ is the Prandtl number, and f is the friction factor expressed as:

$$f = [0.79. \ln Re - 1.64]^{-2} \quad (16)$$

To ensure the validation of the present 2D CFD simulations, comprehensive comparisons between CFD results and theoretical predictions are conducted across varying Reynolds values.

Figure 4 presents a comparison between average

Nusselt numbers obtained from our CFD simulations and theoretical predictions for different Reynolds numbers: $Re = 300, 500, 20000, 50000,$ and 100000 . The first two Reynolds numbers correspond to laminar flow cases with an expected average Nusselt value of 4.36. For the remaining three Reynolds numbers, which represent turbulent flow, the average Nusselt values are calculated using the correlation defined by equations (15) and (16).

As indicated in Figure 4, the results demonstrate strong agreement, confirming the trustworthiness of the 2D CFD approach for both laminar and turbulent cases. The errors observed vary from 0.9% to 10.58%, showcasing the method's reliability in capturing heat transfer behavior in these situations.

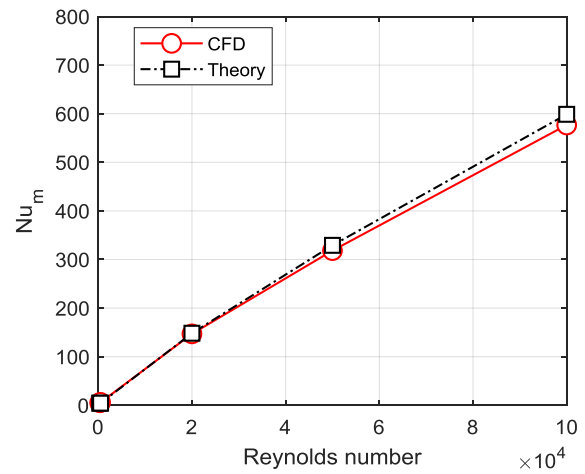


Figure 4. Comparison between CFD simulations and theoretical result for average Nusselt numbers for different Reynolds numbers

Furthermore, Figure 5 showcases the validation of laminar velocity profiles in the fully developed zone, contrasting with the familiar Poiseuille parabolic profile:

$$u = 2U_{in} \left[1 - \left(\frac{r}{R} \right)^2 \right] \quad (17)$$

Despite the robust agreement between CFD and theoretical profiles, it is important to note that for high laminar Reynolds numbers exceeding 500 and less than 2000, the flow does not fully develop within the maximum simulated length of $L = 3$ m. Consequently, to maintain steady-state conditions and adhere to the fully developed regime, laminar Reynolds numbers surpassing 500 have been excluded from this study.

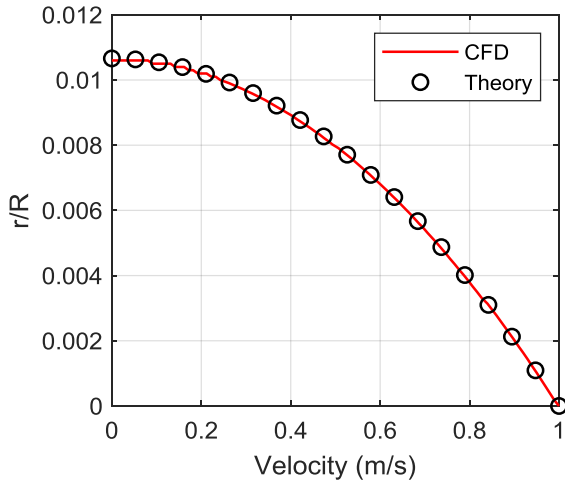


Figure 5. Validation of velocity profile in fully developed zone with laminar parabolic profile, Re =300.

IV.3. Parametric study

• **Effect of receiver tube diameter:**

Figures 6 and 7 depict the evolution of the calculated average Nusselt number along the PTC receiver tube length for various receiver diameters. Figure 6 corresponds to the laminar case (Re = 300), while Figure 7 pertains to the turbulent case (Re = 20000).

The presented figures highlight a consistent trend: in both laminar and turbulent regimes, the average Nusselt number decreases as the PTC receiver diameter increases. Specifically, in the laminar case, a 50% increase in diameter results in an enhancement of approximately 60.03% in the average Nusselt number. Similarly, in the turbulent case, a 50% diameter increase yields a significant rise of 61.42% in the mean Nusselt number. These results underscore the importance of diameter optimization in influencing heat transfer efficiency within the PTC receiver.

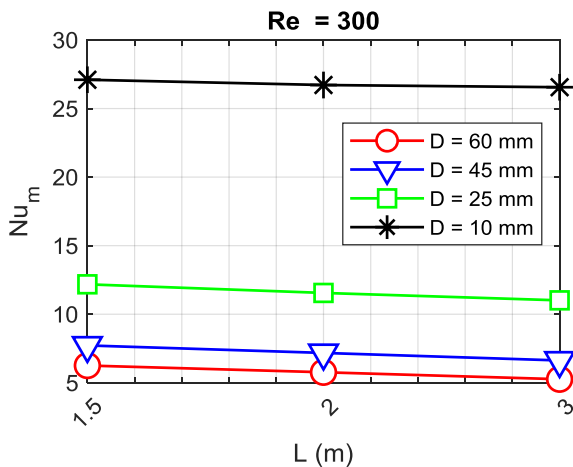


Figure 6. Average Nusselt number vs PTC Receiver length for various PTC receiver diameters at Re = 300

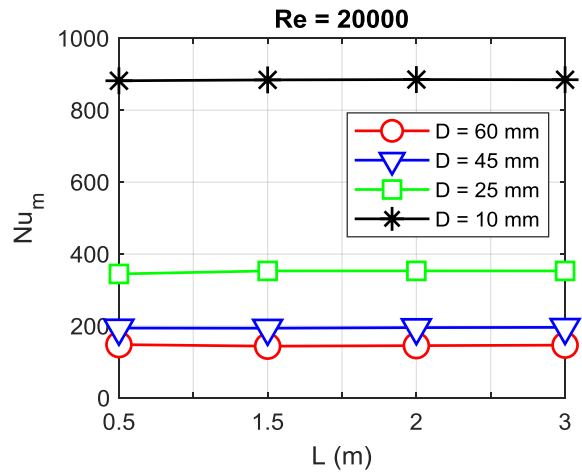


Figure 7. Average Nusselt number vs PTC Receiver length for various PTC receiver diameters at Re = 20000.

• **Effect of receiver tube length**

Figures 8 and 9 depict the change in the calculated average Nusselt number for different PTC receiver tube diameters across various lengths. Figure 8 is associated with the laminar condition (Re = 300), whereas Figure 9 is linked to the turbulent case (Re = 20000). From these figures, it's evident that the impact of the PTC tube length is less significant compared to the PTC tube diameter. In the laminar scenario, a 60% increase in length results in an average percentage decrease of the average Nusselt number by 11.20%, while in the turbulent scenario, it decreases by about 9.93%. Consequently, the effect of length can be considered negligible in comparison to the diameter's influence.

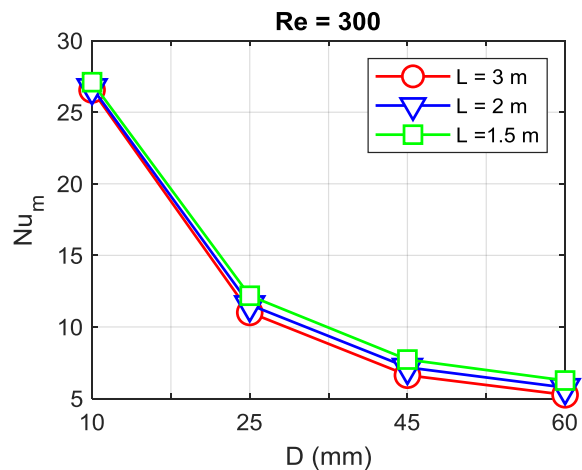


Figure 8. Average Nusselt number vs PTC Receiver diameter for various PTC receiver lengths at Re = 300

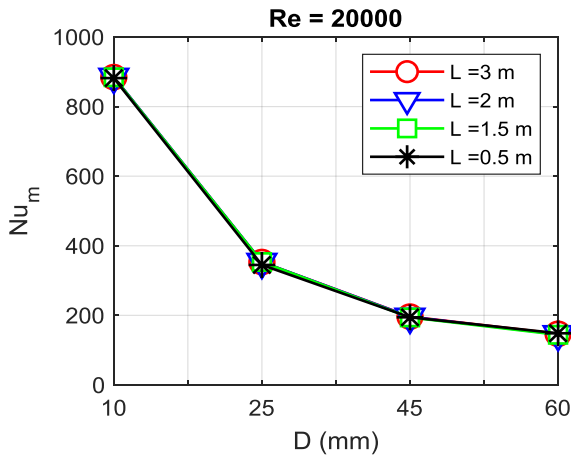


Figure 9. Average Nusselt number vs PTC Receiver diameter for various PTC receiver lengths at Re = 20000.

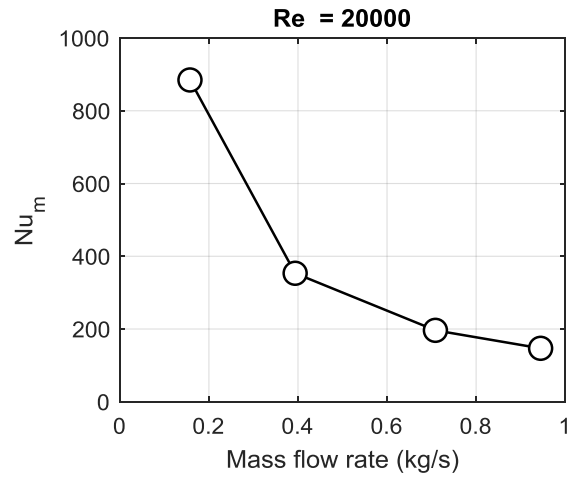


Figure 11. Average Nusselt number vs mass flow rate for turbulent regime, Re = 20000.

• **Effect of Reynolds number and mass flow rate**

The data depicted in Figures 6 through 9 clearly illustrates that the mean Nusselt number holds greater significance in the turbulent case compared to the laminar counterpart. With a substantial increase of 66.66% in Reynolds number, there is a corresponding rise of 30.70% in the average Nusselt number. Consequently, turbulent regimes are strongly recommended for practical applications due to their enhanced heat transfer efficiency.

Figures (10) and (11) show how the mean Nusselt number changes with mass flow rate for laminar and turbulent cases at a constant length of L = 3 m. As mass flow rate increases, both laminar and turbulent flows exhibit a decrease in average Nusselt number. A 60% increase in mass flow rate corresponds to a 50.48% drop in average Nusselt number for laminar flow and a 60.18% decrease for turbulent flow, indicating reduced heat transfer efficiency at higher mass flow rates.

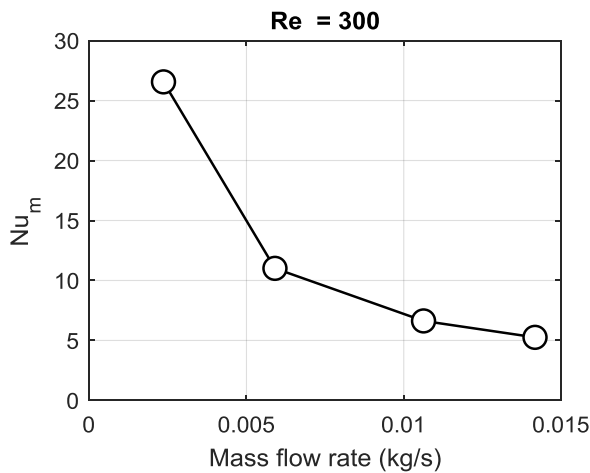


Figure 10. Average Nusselt number vs mass flow rate for laminar regime, Re = 300.

V. Conclusion

This paper introduces 2D steady-state Computational Fluid Dynamics (CFD) simulations to study heat transfer within a Parabolic Trough Collector (PTC) and improve its performance. The study explores different PTC designs, including variations in length (L = 0.5 to 3 m) and diameter (D = 10 to 60 mm), drawn from existing research to enhance PTCs used in desalination systems. The investigation also considers two Reynolds number scenarios for fully developed flows, studying the impact of Reynolds number and mass flow rate. The first step involves a mesh independence study to find a suitable grid for consistent results as the mesh gets finer. A uniform 2 mm spacing in both the x and y directions proves effective for mesh discretization. Following this, the proposed mesh and numerical model are validated using both theoretical and empirical comparisons. The results are evaluated based on the average Nusselt number, which reflects heat transfer efficiency. Higher values indicate better heat exchange performance.

The results obtained can be summarized as follows:

- In both laminar and turbulent regimes, the average Nusselt number decreases as the PTC receiver diameter increases.
- A 50% increase in diameter leads to a 60.03% enhancement in average Nusselt number for laminar flow and a 61.42% rise for turbulent flow.
- The impact of PTC tube length is less significant compared to diameter. A 60% increase in length results in a 11.20% average decrease in laminar case and 9.93% in turbulent case.
- Higher mass flow rates result in decreased average Nusselt numbers for both laminar and turbulent cases.

- A 60% increase in mass flow rate leads to a 50.48% reduction in thermal efficiency for laminar flow and 60.18% for turbulent flow.
- Overall, optimizing PTC receiver diameter is crucial for influencing heat transfer efficiency, while length has a relatively minor effect.

Future endeavors may involve exploring 3D CFD studies under unsteady state conditions and further developing coupled systems that integrate Parabolic Trough Collectors (PTCs) with solar stills.

Declaration

- The authors declare that they have no known financial or non-financial competing interests in any material discussed in this paper.
- The authors declare that this article has not been published before and is not in the process of being published in any other journal.
- The authors confirmed that the paper was free of plagiarism.

References

- [1] International Renewable Energy Agency (IRENA), "Renewable Capacity Statistics", 2021.
- [2] H. Price, E. Lüpfer, D. Kearney, E. Zarza, G. Cohen, R. Gee, R. Mahoney, "Advances in parabolic trough solar power technology", Journal of Solar Energy Engineering Transactions of the ASME, Vol.124, no. 2, 2002, pp 109-125.
- [3] C. Jagadish, A. Biswar, "Modeling and Optimization of Solar Thermal Systems: Emerging research and opportunities", a volume in the Advances in Mechatronics and Mechanical Engineering (AMME) Book Series, IGI Global, US, 2021.
- [4] A. Bellila A. Khechekhouche, I. Kemerchou, A. Sadoun, Antonio Siqueira, N. Smakdji, "Aluminum Wastes Effect on Solar Distillation." ASEAN Journal for Science and Engineering in Materials, Vol. 1, no. 2, 2022.
- [5] A. Khechekhouche, A. M. de Oliveira Siqueira, Nabil Elsharif. "Effect of Plastic Fins on a Traditional Solar Still's Efficiency." International Journal of Energetica, Vol. 7, no. 1, 2022.
- [6] A. Khechekhouche, A. Bellila, A. Sadoun, I. Kemerchou, B. Souyei, N. Smakdji, A. Miloudi, "Iron Pieces Effect on the Output of Single Slope Solar Still." Heritage and Sustainable Development, Vol. 4, no. 2, 2022.
- [7] A. Sadoun, A. Khechekhouche, I. Kemerchou, M. Ghodbane, B. Souyei. "Impact of Natural Charcoal Blocks on the Solar Still Output." Heritage and Sustainable Development, Vol. 4, no. 1, 2022, pp. 61–66.
- [8] A. Brihmat, H. Mahcene, D. Bechki, H. Bouguettaia, A. Khechekhouche, "Energy Performance Improvement of a Solar Still System Using Date and Olive Kernels: Experimental Study." CLEAN - Soil Air Water, December 2022.
- [9] A. Bellila, A., Rahal, Z., Smolyanichenko, A., Sadoun, A. (2023). Cellulose cardboard effect on the performance of a conventional solar still. International Journal of Energetica, Vol.8 , no. 1, pp. doi:http://dx.doi.org/10.47238/ijeca.v5i2.140
- [10] I. Kemerchou, A. Khechekhouche, N. Elsharif, (2023). Effect of Rubber Thickness on the Performance of Conventional Solar Stills under El Oued city climate (Algeria). International Journal of Energetica, Vol.8 , no. 1, pp. 19-23. doi:http://dx.doi.org/10.47238/ijeca.v8i1.212
- [11] A. Khechekhouche, Z. Driss, B.n Durakovic. "Effect of Heat Flow via Glazing on the Productivity of a Solar Still." International Journal of Energetica, Vol. 4, no. 2, 2019, pp. 54-57.
- [12] B. Souyei, A. Khechekhouche, S. Meneceur. "Effect of Comparison of a Metal Plate and a Refractory Plate on a Solar Still." JP Journal of Heat and Mass Transfer, Vol. 27, 2022.
- [13] A. Bellila, B. Souyei and I. Kemerchou, N. Smakdji, A. Sadoun , N. Elsharif, A. Siqueira , "Ethanol Effect on the Performance of a Conventional Solar Still." ASEAN Journal of Science and Engineering, Vol 4, 2022, pp. 25-32. doi: 10.17509/ajse.v4i1.56026
- [14] I. Kemerchou, I. Mahdjoubi, C. Kined, A. Khechekhouche, A. Bellila, G. E. D. Isiordia, "Palm Fibers Effect on the Performance of a Conventional Solar Still." ASEAN Journal For Science And Engineering In Materials, Vol. 1, no. 1, 2022.
- [15] V.E. Dudley, G.J. Kolb, M. Sloan, D. Kearney. "Test results: SEGS LS-2 solar collector", Report of Sandia National Laboratories, 1994.
- [16] H.A. Mohammed, H.B. Vuthaluru, S. Liu, "Parabolic Trough Solar Collectors: Thermal and Hydraulic Enhancement Using Passive Techniques and Nanofluids". Springer Nature, 2022.
- [17] M. Bouhelal, A. Rouag, Y. Belloufi, A. Bouhelal, "Simulation of a Single Slope Solar Still for Clean Water Production in the Ouargla Region of Algeria", Algerian Conference on Mechanics and Solar Energy (ACMSE-2023), Univ of Ouargla, June 2023.
- [18] R. Forristall, "Heat transfer analysis and modeling of a parabolic trough solar receiver implemented in Engineering Solver Equation", Technical report. Colorado, National Renewable Energy Laboratory, 2003.
- [19] O. García-Valladares, N. Velázquez, "Numerical simulation of parabolic trough solar collector: improvement using counter flow concentric circular heat exchangers", Int J Heat Mass Trans, Vol.52, no. 3-4, 2009, pp 597-609.
- [20] A.S. Kalogirou, "A detailed thermal model of a parabolic trough collector receiver". Energy, 48, 2012, pp 298-306.
- [21] O. Al-Oran, F. Lezsovsits, "Recent experimental enhancement techniques applied in the receiver part of the parabolic trough collector–A review", International

- Review of Applied Sciences and Engineering, 2020, Vol. 11, no. 3, pp 209-219.
- [22] C.D. Wilcox, "Review: Turbulence Modelling for CFD". Journal of Fluid Mechanics, 1995, 289, pp 406-407.
- [23] H. Schlichting, "Boundary layer Theory", 7th ed: MCGRAW-HILL Book Company, 1979.
- [24] V. Yakhot, L.M. Smith, "The renormalization group, the ϵ -expansion and derivation of turbulence models". Journal of scientific computing, 7, 1992, pp 35-61.
- [25] ANSYS Fluent documentation, "Fluent Theory Guide", 2016.
- [26] F.P. Incropera, D. P. DeWitt, T. L. Bergman, A. S. Lavine, "Fundamentals of heat and mass transfer", New York: Wiley, 1996.
- [27] V. Gnielinski, "New equations for heat and mass transfer in turbulent pipe and channel flow". International chemical engineering, Vol. 16, no. 2, 1976, pp 359-367.